Planetary and Space Science 57 (2009) 1714–1722

Contents lists available at ScienceDirect

Planetary and Space Science

journal homepage: www.elsevier.com/locate/pss

Plasma in Saturn's nightside magnetosphere and the implications for global circulation

H.J. McAndrews [a,*], M.F. Thomsen [a], C.S. Arridge [b,c], C.M. Jackman [d], R.J. Wilson [a], M.G. Henderson [a], R.L. Tokar [a], K.K. Khurana [e], E.C. Sittler [f], A.J. Coates [b,c], M.K. Dougherty [d]

[a] Space Science and Applications, Los Alamos National Laboratory, P.O. Box 1663, D466, Los Alamos, NM 87545, USA
[b] Mullard Space Science Laboratory, Holmbury St. Mary, Dorking, Surrey, RH5 6NT, UK
[c] Centre for Planetary Sciences at UCL/Birkbeck, University College London, Gower Street, London, WC1E 6BT, UK
[d] Space and Atmospheric Physics Group, Imperial College London, Prince Consort Road, SW7 2BW, UK
[e] Institute of Geophysics & Planetary Physics, University of California, Los Angeles, CA 90095-1567, USA
[f] Heliosphysics Science Division, Geospace Physics Laboratory/Code 673, NASA/Goddard Space Flight Center, 8800 Greenbelt Road, Greenbelt, MD 20771, USA

ARTICLE INFO

Article history:
Received 13 November 2008
Received in revised form
9 February 2009
Accepted 6 March 2009
Available online 17 March 2009

Keywords:
Saturn
Magnetospheric
Ions
Planetary wind
Magnetotail

ABSTRACT

We present a bulk ion flow map from the nightside, equatorial region of Saturn's magnetosphere derived from the Cassini CAPS ion mass spectrometer data. The map clearly demonstrates the dominance of corotation flow over radial flow and suggests that the flux tubes sampled are still closed and attached to the planet up to distances of $50R_S$. The plasma characteristics in the near-midnight region are described and indicate a transition between the region of the magnetosphere containing plasma on closed drift paths and that containing flux tubes which may not complete a full rotation around the planet. Data from the electron spectrometer reveal two plasma states of high and low density. These are attributed either to the sampling of mass-loaded and depleted flux tubes, respectively, or to the latitudinal structure of the plasma sheet. Depleted, returning flux tubes are not, in general, directly observed in the ions, although the electron observations suggest that such a process must take place in order to produce the low-density population.

Flux-tube content is conserved below a limit defined by the mass-loading and magnetic field strength and indicates that the flux tubes sampled may survive their passage through the tail. The conditions for mass-release are evaluated using measured densities, angular velocities and magnetic field strength. The results suggest that for the relatively dense ion populations detectable by the ion mass spectrometer (IMS), the condition for flux-tube breakage has not yet been exceeded. However, the low-density regimes observed in the electron data suggest that loaded flux tubes at greater distances do exceed the threshold for mass-loss and subsequently return to the inner magnetosphere significantly depleted of plasma.

© 2009 Published by Elsevier Ltd.

1. Introduction

When considering the global dynamics of Saturn's magnetosphere, parallels are immediately drawn with the magnetic systems of both Earth and Jupiter. At Earth, the magnetosphere is forced into convective motion by reconnection with the interplanetary field at the dayside magnetopause and the subsequent merging of the opened field lines in the magnetospheric tail. The newly closed field lines rotate back around to the dayside, completing the so-called Dungey cycle (Dungey, 1961).

By contrast, despite evidence for interaction with the solar wind (Walker and Russell, 1985; Khurana, 2001), the fast rotation and significant internal mass-sources in Jupiter's magnetosphere dominate the dynamics of the plasma and fields there. Vasyliunas (1983) described a possible internally driven scenario at Jupiter, in which plasma produced by the moon Io continually loads the magnetic field lines. Due to the interchange process this plasma diffuses outward over many rotations. The filled flux tubes rotate around the dusk magnetosphere, where the reduction in solar wind confinement allows the flux tubes to lengthen. Eventually, the magnetic stress can no longer confine the plasma and the field lines reconnect or break-open to release the plasma downtail as a series of plasmoids in what has previously been termed the "planetary wind" (Michel and Sturrock, 1974). The emptied flux

* Corresponding author. Tel.: +1 505 667 0186; fax: +1 505 665 7395.
E-mail addresses: hazelm@lanl.gov (H.J. McAndrews), mthomsen@lanl.gov (M.F. Thomsen), csa@mssl.ucl.ac.uk (C.S. Arridge), c.jackman@imperial.ac.uk (C.M. Jackman), rjw@lanl.gov (R.J. Wilson), mghenderson@lanl.gov (M.G. Henderson), rlt@lanl.gov (R.L. Tokar), kkhurana@igpp.ucla.edu (K.K. Khurana), Edward.C.Sittler@nasa.gov (E.C. Sittler), ajc@mssl.ucl.ac.uk (A.J. Coates), m.dougherty@imperial.ac.uk (M.K. Dougherty).

0032-0633/$ - see front matter © 2009 Published by Elsevier Ltd.
doi:10.1016/j.pss.2009.03.003

tubes return to the dayside, depleted of plasma, to complete this circulation.

Saturn is also a fast rotator with a large system of rings and moons providing a continual supply of plasma to the magnetosphere through ionisation of neutral gases originating on the rings and moons (Sittler et al., 2004; Tokar et al, 2006), in particular from the active geysers on Enceladus (e.g. Dougherty et al., 2006). At small radial distances the plasma is forced into corotation with the planet (Hill, 1979; Wilson et al., 2008). However, plasma in Saturn's outer magnetosphere is found to be slowed with respect to corotation (Eviatar and Richardson, 1986; Kane et al., 2008). This slowing is indicative of outward plasma transport that leads to subcorotation if the ionosphere is unable to supply enough current to accelerate the plasma to the larger corotation speeds at larger radial distances (Hill, 1979). Furthermore, centrifugal forces stretch the lower-strength magnetic field, until the field lines take the shape of a thin, lagging magnetodisc (Arridge et al., 2006, 2008a) a configuration which lends itself to mass-release via the Vasyliunas or 'planetary wind' model.

In the Saturnian magnetotail the plasma and field properties have been described for several plasmoid-type signatures that were presumably released from mid-tail magnetic reconnection events (Jackman et al., 2007, 2008, submitted; Hill et al., 2008). Only nine such events have been identified to date. In addition to these in-situ observations, remote sensing by the ENA imager detected energetic neutral atoms originating from the tail region between ~20 and 30 R_S suggestive of local acceleration of ions associated with a substorm-type energisation (Mitchell et al., 2005). Furthermore one of these bursts was associated with the in-situ observation of a plasmoid (Hill et al., 2008). Such brightenings in the ENA signature are not uncommon (Carbary et al., 2008) that suggests that the low in-situ detection rate is because Cassini has not been in a favorable viewing location during its excursions into the tail due largely to the warping of the current sheet out of the equatorial plane (Arridge et al., 2008b).

Thus, there is a noteworthy amount of evidence for reconnection-related dynamics in the nightside magnetosphere. Furthermore, the evidence for mass-release in Saturn's magnetosphere is unambiguous; there is no infinite build-up of mass in the system as demonstrated by the relatively stable mass profile in Arridge et al. (2007) which suggests a fairly constant loss rate and by the presence of depleted flux tubes that contain remnants of inner magnetospheric material in the middle and outer magnetosphere.

The principal motivation of the present study is to measure directly the characteristics of the large-scale plasma flows in the nightside magnetosphere to provide insight to the dynamical processes. Are radial flows observed on a large scale both outwards, suggestive of tailward plasma release, and inwards, indicating the return of newly closed field lines? Does the relative density of plasma on these field lines support the idea of plasma release? Can we find evidence of where the Vasyliunas and/or Dungey cycles are closing in the nightside region of the tail? Can we determine whether plasma motions in the tail are governed by solar wind or internal driving?

2. Dataset

2.1. Instrumentation

Plasma parameters are derived from the ion mass spectrometer (IMS) and the electron spectrometer (ELS) that constitute part of the Cassini plasma spectrometer (CAPS) (Young et al., 2004). The IMS provides energy and compositional information for ions with an energy per charge (E/q) of 1 eV/e–50 keV/e using an electrostatic analyser and a subsequent time-of-flight detector. The ELS is an electrostatic analyser with measurement range 0.6 eV/e–28 keV/e. The IMS and ELS fields of view are constructed by sweeping the instrument collection apertures ($160^\circ \times 8.3^\circ$ and $160^\circ \times 5^\circ$ for IMS and ELS, respectively) azimuthally by an actuating platform moving at $\sim 1^\circ\,s^{-1}$. The maximum solid-angle coverage normally allowed by the actuator is $\sim 2\pi$ sr.

One-minute averaged magnetic field data were obtained from the fluxgate magnetometer (FGM) (Dougherty et al., 2004).

2.2. Deriving plasma moments

Moments of the ion distribution (density, temperature and bulk flow velocities) are determined by a process of forward modelling of the assumed convective anisotropic Maxwellian distributions of two species with the same bulk flow velocity (Wilson et al., 2008). The best fit is selected by employing a sequence of minimisation techniques applied to a comparison of the observed and simulated count rate spectrum. It is necessary to pre-select the ion species to be modelled, and for the data shown here we specified a light ion (H^+) and a water group (W^+) component based on lower-resolution time-of-flight measurements of the IMS. Although we assume mass = 17 amu for the heavy ion species, the population may actually include O^+, OH^+, H_2O^+ and H_3O^+ ions, but the derived moments are relatively insensitive to the actual composition. The calculation is carried out over 14×32 s intervals, resulting in ion moments with a ~7 min resolution. Further details regarding the calculation can be found in Tokar et al. (2006) and Wilson et al. (2008).

The electron moments are derived by integrating the particle distribution over three-dimensional velocity space. In general, the electrons have a high thermal speed relative to their bulk speed and so, in the absence of anisotropic pitch-angle distributions, do not have significant directionality. Therefore, the electrons sampled in one direction can generally be considered representative of the local population and in the moment derivation the assumption of isotropy is applied to fill in the section of sky not sampled (Lewis et al., 2008).

The electron spectra are averaged over an actuator cycle, which ranges from ~1 to ~7 min in length, depending on the actuation to remove variability caused by anisotropic variations, and have the background subtracted before integration. Bins with poor signal-to-noise were filtered out before integration to avoid introducing temperature biases to the moments (Arridge et al., 2009).

3. Observations

3.1. Example tail plasma sheet entry

Fig. 1 contains energy–time spectrograms of the ion (top panel) and electron (second panel) data typical of the equatorial magnetotail. These data are from 3 July, 2006, between 0800 and 1200 UT when Cassini was at ~27 R_S and a local time of ~2150. The periodic nature of the ion counts is due to the sweeping of the instrument entrance aperture through the peak of the ion flow, which is strongly directional in the spacecraft frame since the flow speed is comparable to or exceeds the thermal speed. The intermittent presence of the ions in the detector is due to the changing field of view of the instrument relative to the bulk flow direction and this is demonstrated in the field of view plots in a spacecraft-centered frame at the bottom of the figure. The fields of view for the periods corresponding to the red bars on the spectrogram are shown. Between 0900 and 0915 UT the detector is sweeping through the direction of strictly azimuthal flow

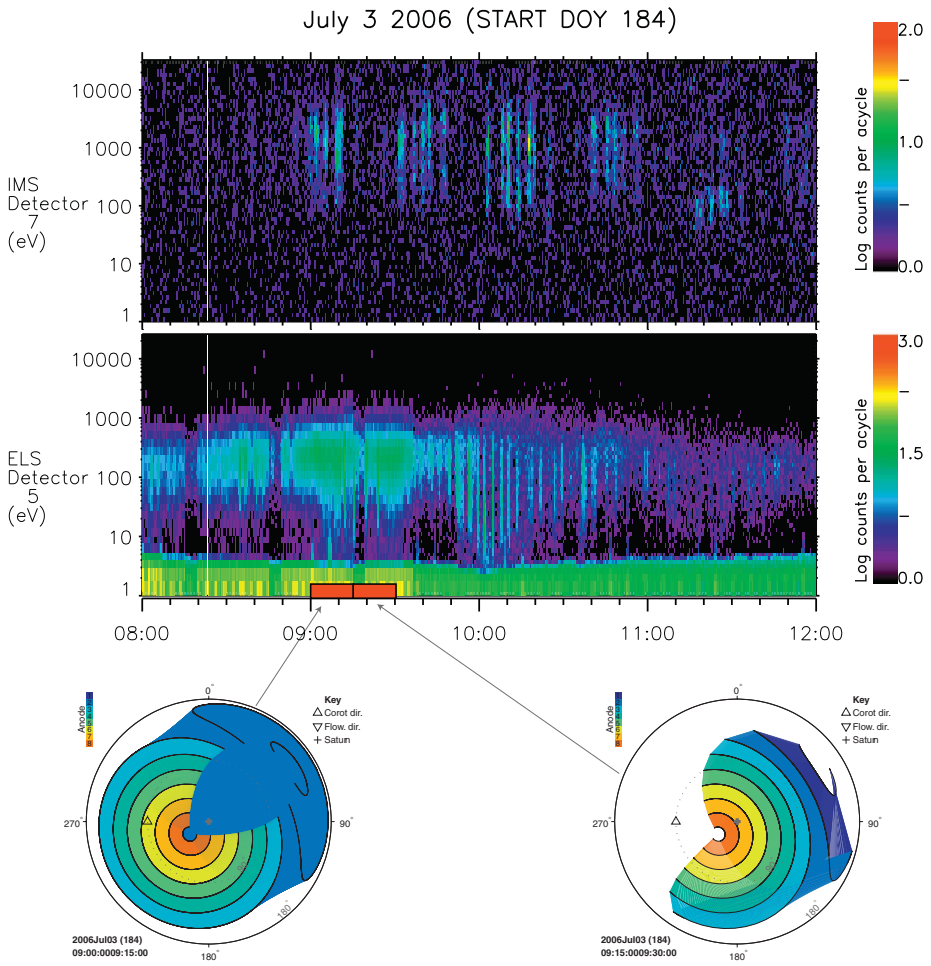

Fig. 1. *Interval on 3 July, 2006*: the top and bottom panels contain time–energy spectrograms from the IMS and ELS instruments on 3 July, 2006. Cassini is at ~27 R_S and at a magnetic local time (LT) of 2150. The colour scale indicates the counts per cycle (32 s); note the different scales for the ions and electrons. The ion spectrogram highlights the low counts and sporadic coverage due to pointing and limited entries into the plasma sheet typical of the tail orbits. Below this are field of view plots for the IMS and ELS during the 15 min intervals indicated by the red bars. The field of view plots are in a spacecraft-centered frame (OAS). The viewing for each polar anode (1–8) is projected onto the sky (note that anode 2 is not displayed on the right-hand figure for clarity). A line from the observer to the centre of the plot is in the direction of positive *S*, (the Cassini to Saturn direction), the north–south direction (O) = $S \times$ (Omega $\times S$) where Omega is Saturn's spin axis and *A* completes the right-handed system. The azimuthal angle is shown on the outside of the outer circle and is about *S*, referenced to zero in the *O* direction. The latitudinal angle is relative to *S* where the inner dashed circle is 90° latitude from *S*. The directions from which strictly corotational and observed flows originate are indicated by a triangle and an upside-down triangle, respectively. Between 0915 and 0930 UT the instrument was not looking into the flow direction, hence the bulk flow vector could not be determined. (For interpretation of the references to colour in this figure legend, the reader is referred to the web version of this article.)

(triangle) and counts are detected allowing us to derive the actual flow direction (upside-down triangle). Note that the actual flow direction is very close to the direction expected for rigidly corotating plasma and indicates the lack of any significant radial flow at this time. In the second case (0915–0930 UT), the actuator does not sweep the instrument through the flow direction and the counts disappear.

The energy structure of the ion counts in the top panel is due to the presence of two main ion populations, a light (primarily H^+) and a heavy (primarily water group, denoted W^+) component, which for the same common flow velocity have energy-per-charge proportional to the ion mass (c.f. Young et al., 2005). In extracting moments these populations must be successfully identified and separated.

These data demonstrate the characteristics of plasma in the outer magnetosphere and highlight the sparse nature of the ions detectable by the IMS. At the start of the interval in Fig. 1, there are no ion counts due to the instrument not sampling the flow direction. The electron counts are low and have energies ~50–500 eV (the intense band of electrons at the lowest energies is due to spacecraft photoelectrons trapped in the potential well surrounding the spacecraft). At ~0900 UT the ions appear as the spacecraft reorients, allowing the IMS to view the flow direction (Fig. 1, bottom left). In this interval the lower energy, light ion peak has energy ~100 eV, and the heavy ion component peaks at ~1000 eV, and has a larger count rate (proportional to energy flux) than the light ions. At the same time the electron counts intensify, and the energy range of the population extends from ~10 to 1000 eV as a lower-energy population is also encountered. There are noticeably higher counts of electrons than ions due to the larger electron flux for a given density and to the larger geometric factor of ELS. Near 1100 UT the electron counts decrease and the energy of the population reverts back to the range ~50–500 eV.

The large-scale variability seen across the whole interval in Fig. 1 is most likely due to the vertical structure of the plasma sheet, observed as the plasma sheet moves up and down across the path of the spacecraft. As is clear from these spectrograms, this structure is not obvious in the ion data. In fact, ions are only

generally seen (when pointing is favourable) at the times corresponding to the regions of highest flux in the electrons, presumably near the centre of the plasma sheet.

3.2. Tail survey

Fig. 2 shows the low-latitude passes from the Cassini orbits from 12 October, 2005 to 24 May, 2007. Between these dates Cassini sampled the equatorial, nightside magnetosphere at a range of planetocentric distances (9–50 R_S) and magnetic local times (2000–0600 MLT).

Intervals to include in the survey were selected based on the criterion that there were sufficient counts on which to perform the ion moments analysis. Since the plasma sheet/magnetodisc is 'pushed' northward out of the equatorial plane, most encounters with it have been found near 10–13° in latitude at ~40 R_S. Because the plasma sheet also exhibits rotational modulation consistent with the planetary spin period (Arridge et al., 2008b) and may flap up and down in response to variations in the solar wind, entries into the plasma sheet are, in practice, sporadic.

The bulk flow of the ions can only be measured if the velocity vector lies within the instrument field of view as demonstrated in Fig. 1. Optimal periods are where the flow is close to the centre of the anode fan and the actuation sweep so that the detector samples the full beam. In total, 35 days between 12 October, 2005 and 24 May, 2007, containing plasma sheet encounters where the IMS was able to sample the peak of the ion flow were collated, providing ~44 h of ion data for use in the tail survey.

In Fig. 3 the derived flow vectors are drawn originating from the spacecraft position at the time of measurement and projected onto the equatorial plane. The vectors are coloured by total ion density ($N_{TOT} = N_{H+}+N_{W+}$). The initial, most striking observation is that the flows in this region are still predominately in the corotational direction, even at large distances from the planet (~50 R_S).

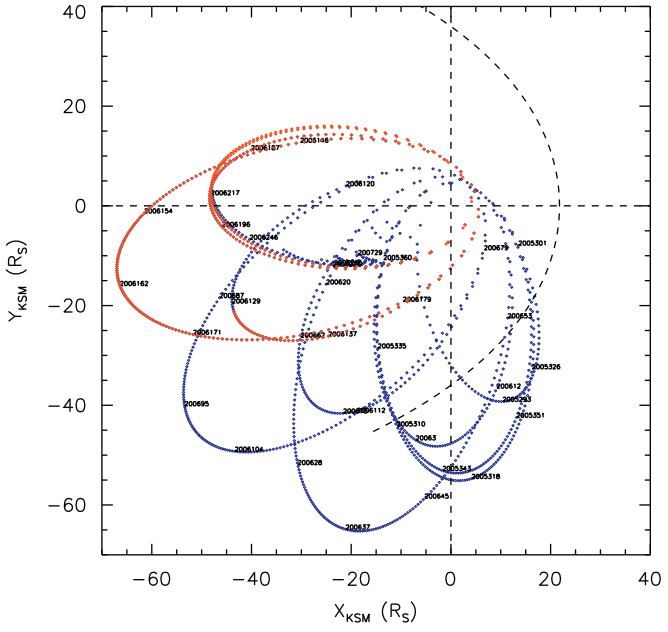

Fig. 2. *Trajectory plot*: trajectory coverage plot for period covered in this study. The blue points denote the orbits surveyed in the ion data. The red points are where both ion and electron data were available. Only electron moments outside of 10 R_S and in the nightside from May 10, 2006 to August 28, 2006 were included in the analysis. (For interpretation of the references to colour in this figure legend, the reader is referred to the web version of this article.)

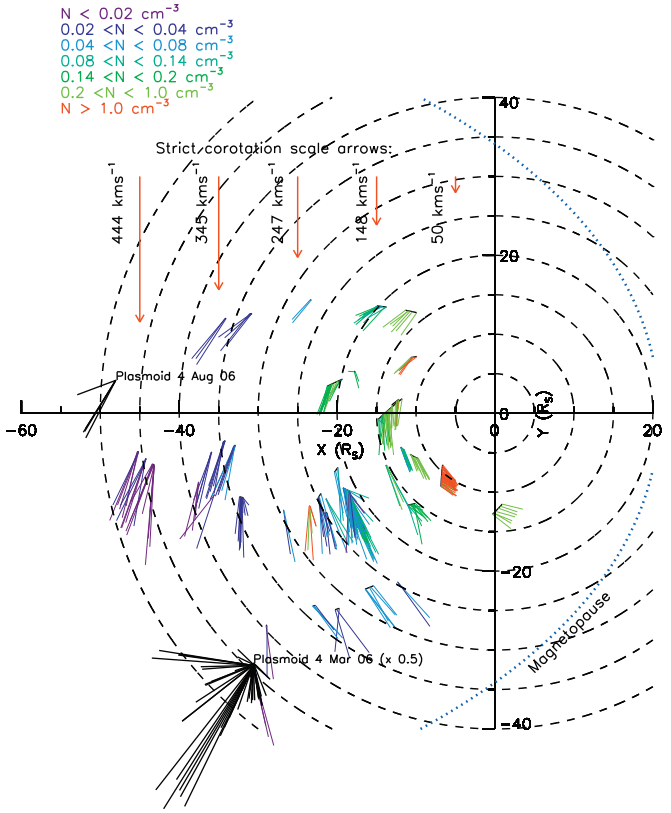

Fig. 3. *Equatorial flow pattern of ions*: the velocity vector of each position was determined using the spacecraft position as the arrow's origin. Arrow length represents velocity and colour the total ion density. Scale arrows for strict corotation at radial distances of 5, 15, 25, 35 and 45 R_S have been indicated along with the magnitude of the corotation speed at that distance. The velocities are in a Saturn-centered equatorial system with the Sun toward the right of the figure. A sample magnetopause surface from Arridge et al. (2006) has been included for context. The flows detected during two plasmoid events on March 4, 2006 and August 4, 2006 (Hill et al., 2008) have been included. Note that the flow speed observed on March 4, 2006 has been scaled down by ~50% relative to the rest of the flows for clarity.

The velocity vectors in Fig. 3 indicate significantly lower flow speeds than the local corotational speed (compare with the scale arrows in Fig. 3) at distances from ~15 R_S outwards. The general flow pattern illustrates the departure from purely azimuthal flow outside of ~20 R_S in the post-midnight sector, where the flow appears to be more dawnward. In this region the flows would not appear likely to circulate on around to the dayside region without a substantial sunward acceleration. There are departures from the purely azimuthal flow with clear instances of more radial flow in agreement with results from Voyager (Lazarus and McNutt, 1983). However, no instances of rapid radial flow, akin to the plasmoid signatures of Hill et al. (2008) (which have been included on the flow pattern for comparison) are observed. Instead, the radial flow is superimposed on the azimuthal flow as a gradual motion of the bulk plasma. There is no notable correlation of density with outwardly moving flows.

Fig. 4 shows several of the derived plasma properties as a function of radial distance from Saturn. In the top panel, the measured azimuthal velocity is plotted and compared with the profile for strictly corotating flow (dashed line). The second panel contains the angle between the direction of bulk and azimuthal flows for each radial distance sampled, with a line at zero marking the transition between inward and outward flow. In the third panel are the proton (green) and water group (red) densities together with the W^+/H^+ density ratio, and the bottom panel

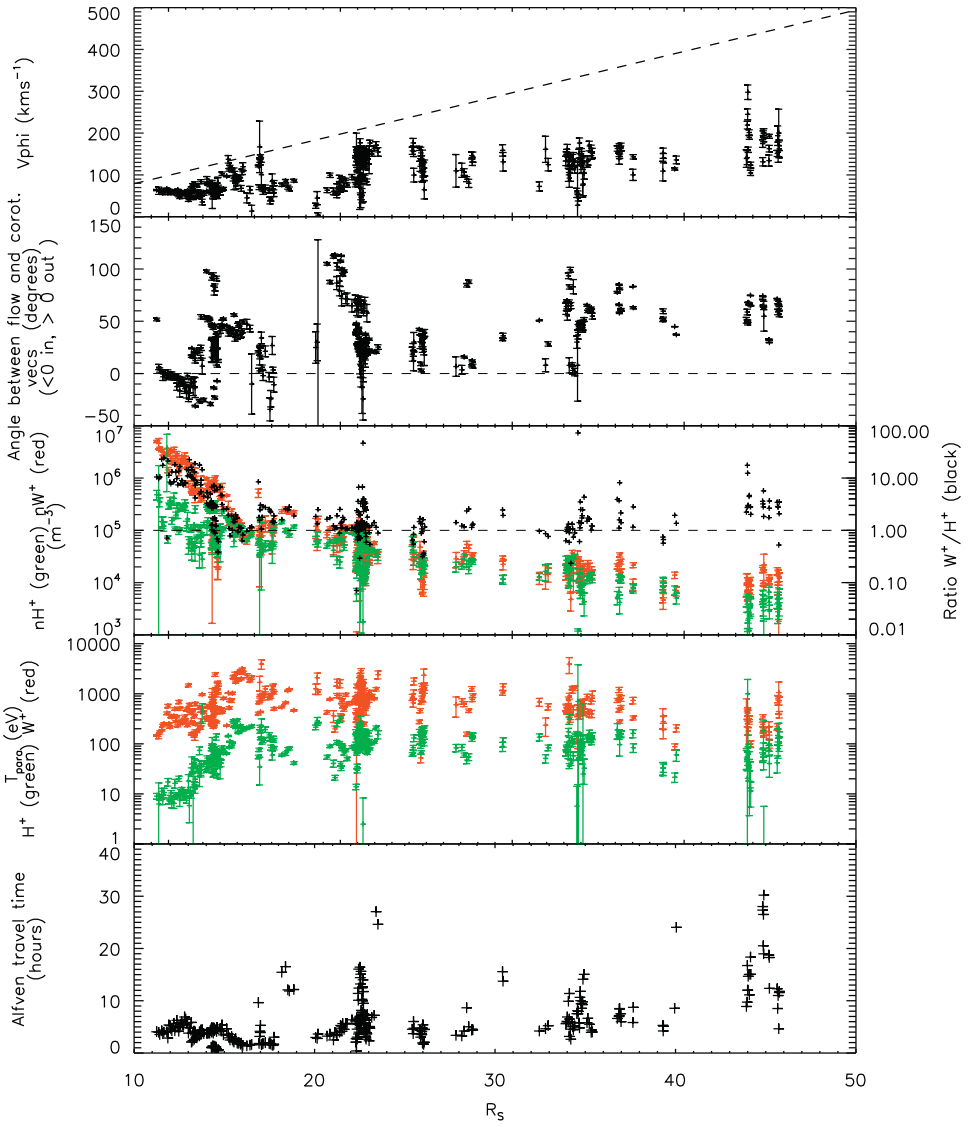

Fig. 4. *Plasma parameters*: (top panel) Vphi vs. *R*, the dashed line is strict corotation, (second panel): the angle of the flow relative to the corotation direction, outward (inward) flows have positive (negative) angles, (third panel) densities for W^+ (red) and H^+ (green) together with the ratio of the heavy-to-light ion densities (black) (fourth panel) parallel temperatures for W^+ (red) and H^+ (green). The errors on the points are an output of the moments code and represent the fitting accuracy obtained, (bottom panel) one-way Alfvén travel time. (For interpretation of the references to colour in this figure legend, the reader is referred to the web version of this article.)

contains the parallel temperatures for the light (green) and heavy (red) ions.

It is clear that the data in all panels of Fig. 4 show a marked change in the nature of the plasma and flows beyond ~15–20 R_S. Outside of 15 R_S the azimuthal velocity no longer increases with radial distance and remains approximately constant at ~100–200 km s^{-1} out to 46 R_S. The azimuthal flow velocities outside of ~25 R_S are in accord with those derived from the MIMI–INCA data (Kane et al., 2008). Azimuthal velocities as low as 0.25 V_{CR} highlight the significant mass-loading on these field lines in agreement with earlier findings (Frank et al., 1980; Richardson, 1986). The subcorotation observed also is in qualitative agreement with the lagging field observed in this region (Arridge et al., 2006).

In general, inward bulk flows are only observed inside of ~15 R_S as demonstrated by the negative angles plotted in the second panel of Fig. 4 inside of this distance. These inward (and outward) motions are most likely the result of global magnetospheric motion.

Outside of 17 R_S, only outward motion is observed, and the flow angle increases with radial distance resulting in more tailward flows (and less strictly azimuthal flows) with increased distance from the planet. Indeed, an examination of the flow pattern in Fig. 3 shows little evidence that the dawn-region flows at larger radial distances will turn sunward and return to the dayside.

Inside of 15 R_S there is a steep drop-off with distance in the densities of both the water group and light ions, although the decline of the density ratio signifies a sharper decrease in the water group ions relative to the light ions. This drop-off is as expected for a dipole field. Outside of 15 R_S the densities of both species decrease comparably with increasing radial distance as evidenced by the flat profile of the density ratio until ~35 R_S when there is a slight increase in the density ratio.

Inside of 15 R_S the parallel ion temperatures (Fig. 4, third panel) increase with radial distance due to the scattering of the pick-up ion population from the inner magnetosphere (e.g. Wilson et al., 2008). Yet once the transition at ~15 R_S is crossed they show an almost constant or slowly declining profile.

In the final panel, we plot the Alfvén travel time to the planet using the local field strength and proton density. The proton density is used since it is representative of the density along the

field line. Values start at sub-1 h increasing to a maximum of 4 h at $>40\,R_S$.

One of the most striking aspects of the ion flow pattern and associated parameters is the lack of inwardly moving flux tubes in the outer magnetosphere. Such motion would be observed if field lines that had recently undergone mass-release were returning to the inner magnetosphere depleted and, due to the reduction of plasma-loading, moving at corotational or possibly even super-corotational speeds. Furthermore, the planetary wind model would favour the release of the most equatorially confined, heavy ions; hence a post-mass-release flux tube should show a preferential depletion of water group ions. The remaining ions would likely have been energised in the magnetic reconnection that produced the mass-release. Hence, one might expect the signature of such returning, depleted flux tubes to be low density, energised, water-depleted ions distributions moving inwards and with faster azimuthal velocities than in the ambient plasma.

No such ion signature is apparent in the intervals sampled. For example, the relatively flat density ratio profile in the third panel of Fig. 4 suggests that no significant water group depletion relative to the light ions is detected. The possible reasons for this are outlined in Section 3.3.

3.3. Why are return flows not observed in the ion data?

The lack of signatures of returning, depleted flux tubes in the intervals represented by Figs. 3 and 4 could arise if (a) there is no such inward flow in the region sampled, (b) the inflow channels are physically much narrower in azimuth than the outflow channels (Chen and Hill, 2008), which makes them less likely to be included in this dataset, (c) the IMS is never orientated such that it is looking outward to detect inward flows or (d) the low density, energised, post-reconnection ions have fluxes too low to be detectable by the IMS. The look direction plots in Fig. 1 demonstrate the situation in case (c), where the bottom left shows an interval with nearly complete viewing of the sky, but the bottom right plot shows the pointing for an interval only sampling a portion of the sky and where inflows could be missed.

In case of (c), we can establish whether instrument pointing introduces a bias into the results by comparing how often the IMS is sampling each direction and the percentage of inward or outward flows detected. In Table 1 are the durations of the look and flow directions observed for inward and outward flows outside of $22\,R_S$. In this region of the outer magnetosphere, according to Fig. 3, almost no inward flows are observed. The percentage of inward flows detected relative to the time the instrument is looking outward is very small and in fact can be attributed to one single data point. Upon further inspection there is no noticeable difference between this data point and the surrounding ones and it may be a spurious result. Nevertheless, it is clear that the IMS has plenty of opportunity to sample inward flows (it is looking outward for 7 h of the total time), yet none are seen. Conversely, when the instrument looks inward, an abundance of outward flows are detected.

Table 1
Duration of inward- and outward-flow detection beyond $22\,R_S$.

Instrument look (plasma flow) direction	Look time (of 13 h in total) (h)	Duration of observed flows (h)	Duration of flows seen as a percentage of opportunities (%)
Outward (inward)	7	0.2	0.02
Inward (outward)	13	12.8	98.0

Instrument look directions. The inward and outward look durations are calculated from the percentage of time within one sampling period (14×32 s) that the instrument is looking inward or outward. The sum of these percentages is greater than 100%, because the instrument can often see both inward and outward flow directions within a sampling period. For this calculation we make the assumption that the radial flow component from the moment calculations within that sampling period is constant within a sampling interval. This could smooth out short-duration radial motion. Only periods outside of $22\,R_S$ have been considered.

In case of (d) we employ the ELS data, with its greater detection sensitivity, to characterise the electrons in the regions sampled. This will establish whether the IMS is effectively 'blind' to such a low-density population. For this purpose electron densities for all passes into the magnetotail plasma sheet outside of $\sim10\,R_S$ from May 10, 2006 to August 28, 2006 (Fig. 2) were used in addition to those dates corresponding to the ion events shown in Fig. 3.

We first compare the ion and electron densities from the tail in Fig. 5. We limit the electron density used to values $>10^3\,m^{-3}$, since densities below this most likely correspond to lobe measurements (Arridge et al., submitted). The ELS densities are shifted by an empirically determined factor to make them agree with the ion densities when both are measured. There is a lack of low-density points in the ion data set at low radial distances ($<20\,R_S$); this can be attributed to a selection effect. At low radial distances there are more intervals with higher fluxes which are selected for the survey in preference to the lower flux events.

Fig. 5 shows that the ion densities derived for the intervals presented in Figs. 3 and 4 are essentially all near the upper edge of the range of electron densities at any given radial distance. We attribute this to the lower sensitivity of ion detection, with the abundant presence of lower electron densities revealing an additional, lower-density population unseen in the IMS data and potentially representing the anticipated depleted flux tubes returning to the inner magnetosphere. There is no clear correlation of the low-density electron regions with local time or radial distance, suggesting that if these are signatures of the mass-release processes, then it occurs across the whole region sampled and not preferentially in the dusk magnetosphere as proposed by Vasyliunas (1983) and Cowley et al. (2004).

Ion densities of two of the plasmoid events identified in Jackman et al. (2007) and Hill et al. (2008) (March 4, 2006 and August 4, 2006) are also included in Fig. 5 (squares). The plasmoid densities for the first case have a range of values, extending to very low values at the very limit of what can be observed in the IMS. For the second case, the densities are near the top of the maximum values detected in this region. Therefore, were Cassini

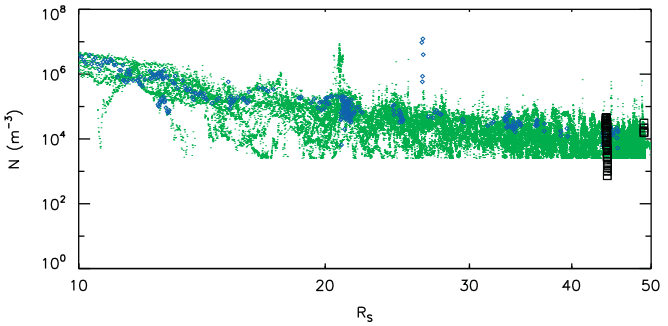

Fig. 5. *Density with distance from the planet and the centre of the current sheet*: total ion density (H^+ and W^+) (blue) over plotted on the corrected electron density (green) against radial distance. The ion density of two of the plasmoid events from Jackman et al. (2007) and Hill et al. (2008) are plotted as black squares ($44\,R_S$: March 4, 2006 and $49\,R_S$: August 4, 2006). Densities $<2.5\times10^3\,m^{-3}$ are not included as they are assumed to be lobe regions. Ions are only detected above a limiting density (which is R dependent). However, electrons are detected at densities lower than this. (For interpretation of the references to colour in this figure legend, the reader is referred to the web version of this article.)

in a favorable position on the dates included in this survey, to detect passing plasmoids, we would expect to detect them. Positive identification of the plasmoids in the studies of Jackman et al. (2007, 2008) and Hill et al. (2008) was achieved using magnetic field data. A sharp, northward-turning of the primarily southward-pointing planetary field indicates that the field lines have moved from a stretched- to a plasmoid-type configuration, yet no such magnetic signatures have been associated with any of the intervals in this study, which all appear to be on closed field lines. Furthermore, during none of the events studied here is there evidence for a large rotation of the velocity from a largely azimuthal flow direction to a strongly tailward flow, also indicative of plasmoid release (Hill et al., 2008), and, thus we conclude that despite similarities in density, the events included in this study are not plasmoid signatures and are still on closed field lines attached to the planet.

4. Discussion

4.1. Saturn's magnetospheric tail

From the ion moments computed from IMS measurements, complemented and enhanced by those from the ELS dataset, the following picture emerges regarding Saturn's magnetospheric tail:

In the outer magnetosphere ($\sim>20\,R_S$) the plasma and flows are markedly different from those observed inside of $20\,R_S$. We find the magnetotail plasma sheet to be a water group-laden region that is still circulating at $50\,R_S$ downtail with a large dawnward component to the flow pattern. The significant corotational component, even in the distant tail ($\sim 50\,R_S$), indicates that the magnetosphere can contain the plasma pressure out to large distances. However, the level of subcorotation is a signature that Saturn's ionosphere is unable to enforce full corotation on the mass-loaded field lines. It follows that the plasma must be flowing outward and the slow-down is a result of the conservation of angular momentum. Although we see evidence of mass moving radially outward generally, there is no clear evidence for the dynamic process that should ultimately result in the loss of mass from the system of closed field lines, nor the return of magnetic flux to the inner magnetosphere required due to flux conservation. As described in Section 3.3 there are a number of selection criteria that mitigate against observing such features, namely the small scale-size of the inflow channels (Chen and Hill, 2008), the low density expected in returning flux tubes and the likelihood of favourable instrument viewing.

The flow pattern indicates that the observed flux tubes are likely to encounter the dawn magnetopause, as the strongly dawnward flow observed implies; however, measurements adjacent to the dawn magnetopause do not indicate a large build-up of plasma. Thus the plasma either manages to rotate around dawn to the dayside, or it is lost either downtail into interplanetary space.

The striking change in the characteristics of the plasma sheet beyond $\sim$15–$20\,R_S$ is most likely due to the transition from the region dominated by closed flux tubes that are able to complete an entire rotation of the planet (closed drift path), and the outer magnetospheric flux tubes which may not remain closed as they convect through the tail due to the centrifugal stresses brought on by significant mass-loading. We also note that this is just inside the expected hinging distance of the magnetotail current sheet (Arridge et al., 2008b) and where the field lines start to become significantly stretched.

The Alfvén travel times in Fig. 4 are shown to increase with radial distance. Travel times of a few hours are consistent with a slight delay in the communication between the distant field line and the ionosphere resulting in the corotation lag observed. Beyond $40\,R_S$ travel times of up to 4 h are observed, consistent with the increasing dawnward component of the flow shown in Figs. 3 and 4.

We underline that the analysis here has not indicated whether solar wind driving is instrumental in the motions of the outer magnetospheric plasma. With a detailed compositional analysis, it may be possible to distinguish flux tubes populated by solar wind plasma (He^{++}) via dayside (or nightside) reconnection, from flux tubes containing heavy ions with an origin in the inner magnetosphere. Due to the ubiquitous presence of water group ions, all the relatively dense intervals analysed here will fall into the latter category.

Finally, we have identified a lower-density population revealed by the electron observations at all radial distances and local times, which may include signatures of returning flux tubes, although we are unable to derive their motion.

4.2. Flux-tube content and threshold for field-breaking

We can attempt to characterise any mass-loss by estimating the flux-tube content versus radial distance in the region of the magnetosphere sampled. The flux-tube content, in the absence of sources and sinks, is conserved for a given flux tube during the outward transport process (Hill and Dessler, 1976), and is $\eta \equiv \int (n(s)/B(s))ds$, where the integral is taken along a field line. We can approximate this integral as $\eta = \int (n(s))/B(z(s))ds$, where $n(z(s)) = n_0 \exp(-W/kT)$, n_0 is the equatorial density and T the parallel ion temperature (both derived from the IMS data), W is the centrifugal potential and $B(z(s))$ corresponds to the field strength derived from the magnetospheric field model of Khurana et al. (2006). The centrifugal potential is derived using the assumption that a single field line rotates with the same level of subcorotation as measured at the equator. Since we derive equatorial azimuthal velocities we can work out the fraction of subcorotation, f and use $W = 0.5mf^2r^2\Omega^2$. The distance along the field line, ds is derived assuming a parabolic-shaped field line in the stretched field region and we multiply the values by the mass in kg to get the flux-tube mass content plotted in the top panel of Fig. 6 (diamonds). There is significant spread in the data at all values of R, indicative of the varying flux tube volumes encountered in the tail, presumably due to the cycle of mass-release and loading. The values show a slight decrease with radial distance, in particular the upper limit of the distribution of points decline with R. This suggests that despite the requirement that under no mass-loss the flux tube content is preserved, there is a loss of flux tubes with a high mass content (at the upper limit of the profile) with increasing R. Thus, those are lost downtail and what we are effectively seeing are the "survivors" of the mass-loss process or Vasyliunas cycle. Despite the paucity of data points between $\sim$25–$35\,R_S$, and 35–$43\,R_S$ there is a rather invariant width to the distribution of points. The constant spread of points indicates that the flux tube content is, in general, preserved, but it cannot be preserved for those above a certain limit.

We can quantify this limit by testing whether the flux tube content observed is theoretically sufficient to break-open the magnetic field in the tail. This breaking limit is achieved when the mass per unit flux η, exceeds a critical limit related to the tail field, B_T: $\eta > B_T r/\mu_0 V_\Phi^2$ (Goertz, 1983), where B_T is the value of the lobe field strength above and below the plasma sheet at that distance. The lobe field strength is obtained from values corresponding to those points at which the density is $<10^3\,\mathrm{m}^{-3}$.

To apply this criterion to Saturn's tail, we use the values for η in the top panel of Fig. 6 and over plot the estimated critical limit for

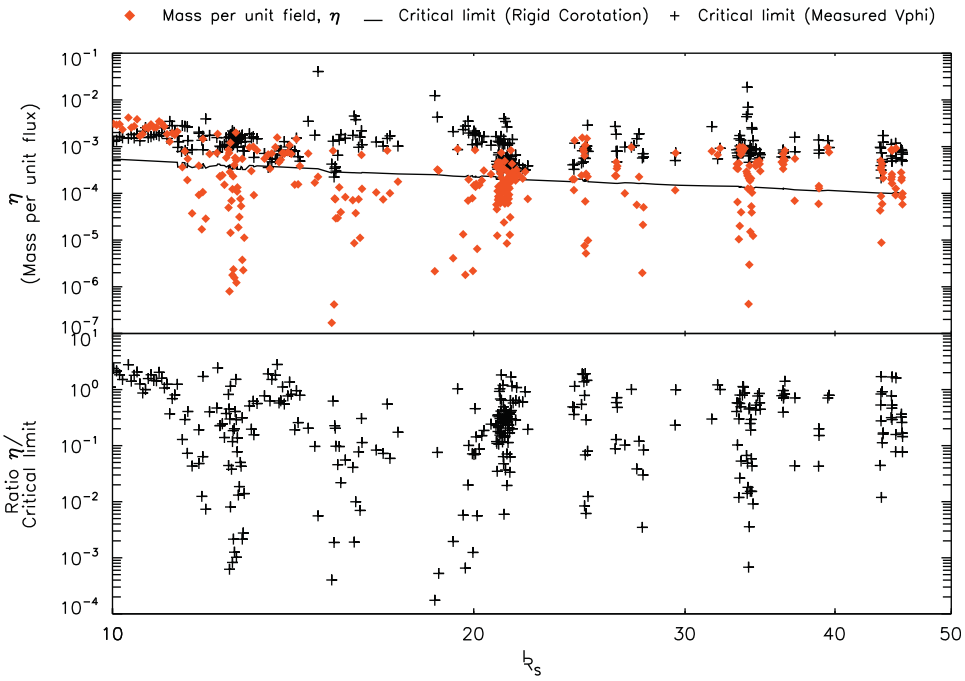

Fig. 6. *Flux tube content and mass-release criteria*: (top panel) The measured mass per unit flux tube, η (diamonds) compared with the theoretical 'critical limit' (Goertz, 1983) beyond which a flux tube will undergo pinch off and release the plasma downtail. This limit is shown for both strict corotation (solid line) and the actual measured values of azimuthal velocity (crosses). (Bottom panel) the ratio of η to the critical limit for the observed flow.

strict corotation (solid line) and the observed subcorotation (crosses). If the plasma were strictly corotating some of the measured intervals would exceed the critical value. However, the slowing of the flux tubes allows them to circulate through the tail without the need to release plasma since the measured flux tube contents are well below the theoretical limit for field-breaking. In the second panel is the ratio of the mass per unit flux to the critical limit which is approximately level.

4.3. Triggering mass-loss processes/drivers of tail reconnection

As we have shown, heavily loaded, stretched flux tubes may undergo mass-release in the tail if some threshold relating to the mass-loading rate and field strength is reached. However, it is possible that an alternative trigger may initiate the pinch-off process. For example, Bunce et al. (2005) described an energetic particle event observed in the magnetotail during SOI and attributed it to tail reconnection instigated by magnetospheric compression by a solar wind corotating interaction region (CIR). Russell et al. (2008) found that four of the five substorm events identified in Jackman et al. (2008) were triggered when Titan was within one Saturn rotation of the highly stretched tail field lines at midnight local time.

We have not considered the effects of the external solar wind conditions or the position of Titan during the events studied here; however, we propose that in cases of fast rotation, coupled with sufficient mass build-up, field lines can reconnect across the stretched current sheet and drive plasmoid formation without, necessarily, an external driver. This agrees with the proposal by Hill et al. (1974) and more recent work by Russell et al. (2008) that state that due to the inefficiency of the reconnection process at Saturn's dayside magnetosphere, accumulation of mass in the tail flux tubes may dominate plasmoid formation, not closure of open flux generated at the dayside magnetopause.

5. Conclusions

We have used ion moment data from the Cassini-IMS instrument to describe the nature of the plasma sheet dynamics in the Saturnian magnetotail. The corotational flow suggests there is a population which is most likely on closed field lines still rotating with the planet, albeit at a slower rate due to the heavy load. The ubiquitous presence of water group ions, together with the constancy of the amount of water group ions relative to light ions implies that mass-release has not occurred for the intervals for which we have derived ion parameters, since we would expect the preferential release of the equatorially confined heavy species. Such a mass-laden state represents flux tubes that are not yet ready to break-off and release plasma downtail, though they may yet do so at greater distances since we find little evidence for their return to the dayside. Through theoretical considerations we strengthen the case for these flux tubes having survived their passage through the tail because the centrifugal force on the plasma sheet is not large enough to exceed the restraining tension in the magnetic field and break it open to release the plasma (Vasyliunas, 1983). The low-density electrons have revealed a population which may well be the return flow from mass-release processes in the tail; however, these intervals are too tenuous to produce detectable ions, and therefore by default excluded from our analysis. We note that these depleted plasma sheet regions are seen at all radial distances and no clear local time dependency in the nightside is found agreeing with Chen and Hill (2008).

Acknowledgements

The work at Los Alamos was performed under the auspices of the US DOE and was supported by the NASA Cassini program. Work at Southwest Research Institute was supported by the JPL Contract 1243218. Cassini is managed by the Jet Propulsion Laboratory for NASA. Work at Imperial was supported by the STFC

C.S.A. and A.J.C. were supported in this work by the STFC rolling grant to MSSL/UCL. Part of this work was discussed during a team meeting at the International Space Science Institute in Bern, Switzerland. HJM, MFT, CSA and ECS acknowledge funding from ISSI to attend this meeting.

References

Arridge, C.S., Achilleos, N., Dougherty, M.K., Khurana, K.K., Russell, C.T., Southwood, D.J., Cassini MAG Team, 2006. The configuration of Saturn's magnetosphere as observed by the Cassini magnetometer. Eos Trans. AGU 87 (36) (Jt. Assem. Suppl., Abstract P43B-06).

Arridge, C.S., Russell, C.T., Khurana, K.K., Achilleos, N., André, N., Rymer, A.M., Dougherty, M.K., Coates, A.J., 2007. Mass of Saturn's magnetodisc: Cassini observations. Geophys. Res. Lett. 34, L09108.

Arridge, C.S., Russell, C.T., Khurana, K.K., Achilleos, N., Cowley, S.W.H., Dougherty, M.K., Southwood, D.J., Bunce, E.J., 2008a. Saturn's magnetodisc current sheet. J. Geophys. Res. 113, A04214.

Arridge, C.S., Khurana, K.K., Russell, C.T., Southwood, D.J., Achilleos, N., Dougherty, M.K., Coates, A.J., Leinweber, H.K., 2008b. Warping of Saturn's magnetospheric and magnetotail current sheets. J. Geophys. Res. 113, A08217.

Arridge, C.S., Gilbert, L.K., Lewis, G.R., Sittler, E.C., Jones, G.H., Kataria, D.O., Coates, A.J., Young, D.T., 2009. The effect of spacecraft radiation sources on electron moments from the Cassini CAPS Electron Spectrometer, Planet. Space Sci., in press, doi:10.1016/j.pss.2009.02.011.

Arridge, et al., Plasma electrons in Saturn's magnetotail: structure, distribution and Energisation. Planet. Space Sci., submitted.

Bunce, E.J., Cowley, S.W.H., Wright, D.M., Coates, A.J., Dougherty, M.K., Krupp, N., Kurth, W.S., Rymer, A.M., 2005. In situ observations of a solar wind compression-induced hot plasma injection in Saturn's tail. Geophys. Res. Lett. 32, L20S04.

Carbary, J.F., Mitchell, D.G., Brandt, P., Roelof, E.C., Krimigis, S.M., 2008. Statistical morphology of ENA emissions at Saturn. J. Geophys. Res. 113, A05210.

Chen, Y., Hill, T.W., 2008. Statistical analysis of injection/dispersion events in Saturn's inner magnetosphere. J. Geophys. Res. 113, A07215.

Cowley, S.W.H., Bunce, E.J., Prangé, R., 2004. Saturn's polar ionospheric flows and their relation to the main auroral oval. Ann. Geophys. 22, 1379–1394.

Dougherty, M.K., et al., 2004. The Cassini magnetic field investigation. Space Sci. Rev. 114, 331–383.

Dougherty, M.K., Khurana, K.K., Neubauer, F.M., Russell, C.T., Saur, J., Leisner, J.S., Burton, M.E., 2006. Identification of a dynamic atmosphere at Enceladus with the Cassini magnetometer. Science 311 (5766), 1406–1409.

Dungey, J.W., 1961. Interplanetary magnetic field and the auroral zones. Phys. Rev. Lett. 6, 48–49.

Eviatar, A., Richardson, J.D., 1986. Corotation of the Kronian magnetosphere. J. Geophys. Res. 91 (A3), 3299–3303.

Frank, L.A., Burek, B.G., Ackerson, K.L., Wolfe, J.H., Mihalo, J.D., 1980. Plasma's in Saturn's magnetosphere. J. Geophys. Res. 85 (A11), 5696–5708.

Goertz, C.K., 1983. Detached plasma in Saturn's front side magnetosphere. Geophys. Res. Lett. 10 (6), 455–458.

Hill, T.W., 1979. Inertial limit on corotation. J. Geophys. Res. 83 (A11), 6554–6558.

Hill, T.W., Dessler, A.J., Michel, F.C., 1974. Configuration of the Jovian magnetosphere. Geophys. Res. Lett. 1, 3.

Hill, T.W., Dessler, A.J., 1976. Longitudinal asymmetry of the Jovian magnetosphere and the periodic escape of energetic particles. J. Geophys. Res. 81 (19), 3383–3386.

Hill, T.W., Thomsen, M.F., Henderson, M.G., Tokar, R.L., Coates, A.J., McAndrews, H.J., Lewis, G.R., Mitchell, D.G., Jackman, C.M., Russell, C.T., Dougherty, M.K., Crary, F.J., Young, D.T., 2008. Plasmoids in Saturn's magnetotail. J. Geophys. Res. 113, A01214.

Jackman, C.M., Russell, C.T., Southwood, D.J., Arridge, C.S., Achilleos, N., Dougherty, M.K., 2007. Strong rapid dipolarizations in Saturn's magnetotail: in situ evidence of reconnection. Geophys. Res. Lett. 34, L11203.

Jackman, C.M., Arridge, C.S., Krupp, N., Bunce, E.J., Mitchell, D.G., Kurth, W.S., McAndrews, H.J., Dougherty, M.K., Russell, C.T., Achilleos, N., Coates, A.J., Jones, G.H., 2008. A multi-instrument view of tail reconnection at Saturn. J. Geophys. Res.

Jackman, C.M., Lamy, L., Freeman, M.P., Zarka, P., Cecconi, B., Kurth, W.S., Cowley, S.W.H., Dougherty, M.K., On the character and distribution of lower-frequency radio emissions at Saturn, and their relationship to substorm-like events, JGR, submitted.

Kane, M., Mitchell, D.G., Carbary, J.F., Krimigis, S.M., Crary, F.J., 2008. Plasma convection in Saturn's outer magnetosphere determined from ions detected by the Cassini INCA experiment. Geophys. Res. Lett. 35, L04102.

Khurana, K.K., 2001. Influence of solar wind on Jupiter's magnetosphere deduced from currents in the equatorial plane. J. Geophys. Res. 106, A11.

Khurana, K.K., Arridge, C.S., Schwarzl, H., Dougherty, M.K., 2006. A model of Saturn's magnetospheric field based on latest Cassini observations. Eos Trans. AGU 87 (36) (Jt. Assem. Suppl., Abstract P44A-01).

Lazarus, A.J., McNutt, R.L., 1983. Low energy plasma ion observations in Saturn's magnetosphere. J. Geophys. Res. 88, 8831.

Lewis, G.R., André, N., Coates, A.J., Gilbert, L.K., Linder, D.R., Rymer, A.M., 2008. Derivation of density and temperature from the Cassini—Huygens CAPS electron spectrometer. Planet. Space Sci. 56 (7), 901–912.

Michel, F.C., Sturrock, P.A., 1974. Centrifugal instability of the Jovian magnetosphere and its interaction with the solar wind. Planet. Space Sci. 22 (11), 1501–1510.

Mitchell, D.G., Brandt, P.C., Roelof, E.C., Dandouras, J., Krimigis, S.M., Mauk, B.H., Paranicas, C.P., Krupp, N., Hamilton, D.C., Kurth, W.S., Zarka, P., Dougherty, M.K., Bunce, E.J., Shemansky, D.E., 2005. Energetic ion acceleration in Saturn's magnetotail: substorms at Saturn? Geophys. Res. 32, L20S01.

Richardson, J.D., 1986. Thermal ions at Saturn: plasma parameters and implications. J. Geophys. Res. 91, 1381.

Russell, C.T., Jackman, C.M., Wei, H.Y., Bertucci, C., Dougherty, M.K., 2008. Titan's influence on Saturnian substorm occurrence. Geophys. Res. Lett. 35, L12105.

Sittler, E.C., Johnson, R.E., Jurac, S., Richardson, J.D., McGrath, M., Crary, F., Young, D.T., Nordholt, J.E., 2004. Pickup ions at Dione and Enceladus: Cassini plasma spectrometer simulations. J. Geophys. Res. 109, A01214.

Tokar, R.L., Johnson, R.E., Hill, T.W., Pontius, D.H., Kurth, W.S., Crary, F.J., Young, D.T., Thomsen, M.F., Reisenfeld, D.B., Coates, A.J., Lewis, G.R., Sittler, E.C., Gurnett, D.A., 2006. The interaction of the atmosphere of Enceladus with Saturn's plasma. Science 311, 1409–1412.

Vasyliunas, V.M., 1983. Plasma distribution and flow. In: Dessler, A.J. (Ed.), Physics of the Jovian magnetosphere. Cambridge planetary science series.

Walker, R.J., Russell, C.T., 1985. Flux transfer events at the Jovian magnetopause. J. Geophys. Res. 90 (A8), 7397–7404.

Wilson, R.J., Tokar, R.L., Henderson, M.G., Hill, T.W., Thomsen, M.F., Pontius Jr., D.H., 2008. Cassini plasma spectrometer thermal ion measurements in Saturn's inner magnetosphere. J. Geophys. Res. 113, A12218.

Young, D.T., et al., 2004. The Cassini plasma spectrometer investigation. Space Sci. Rev. 114, 1–112.

Young, D.T., et al., 2005. Composition and dynamics of plasma in Saturn's magnetosphere. Science 307 (5713), 1262–1266.